Thermochromic and Mechanochromic Luminescence Umpolung in Isostructural Metal–Organic Frameworks Based on Cu6I6 Clusters

ARTICLE *in* INORGANIC CHEMISTRY · JANUARY 2015

Impact Factor: 4.76 · DOI: 10.1021/ic502207f

4 AUTHORS:

Mahesh Sadashiv Deshmukh
Indian Institute of Science Education and Res…
1 PUBLICATION **5** CITATIONS
SEE PROFILE

Ashok Yadav
Indian Institute of Science Education and Res…
6 PUBLICATIONS **7** CITATIONS
SEE PROFILE

Rakesh Pant
Indian Institute of Science Education and Res…
2 PUBLICATIONS **5** CITATIONS
SEE PROFILE

Ramamoorthy Boomishankar
Indian Institute of Science Education and Res…
46 PUBLICATIONS **952** CITATIONS
SEE PROFILE

Inorganic Chemistry

Article

pubs.acs.org/IC

Thermochromic and Mechanochromic Luminescence Umpolung in Isostructural Metal–Organic Frameworks Based on Cu_6I_6 Clusters

Mahesh S. Deshmukh, Ashok Yadav, Rakesh Pant, and Ramamoorthy Boomishankar*

Department of Chemistry, Indian Institute of Science Education and Research (IISER), Pune, Dr. Homi Bhabha Road, Pune 411008, India

Supporting Information

ABSTRACT: Two isostructural metal–organic framework (MOF) materials, namely, $\{[MeSi(^3Py)_3]_6(Cu_6I_6)\}_n$ (**1**) and $\{[\ MeSi(^3Qy)_3]_6(Cu_6I_6)\}_n$ (**2**), featuring Cu_6I_6 clusters were synthesized from tridentate arylsilane ligands of the type $MeSi(^3Py)_3$ (^3Py = 3-pyridyl) and $MeSi(^3Qy)_3$ (^3Qy = 3-quinolyl), respectively. While the MOF **1** displays the usual thermochromism associated with traditional $Cu_4I_4Py_4$ clusters, the MOF **2** shows ^{3}XLCT/^{3}MLCT emission due to the Cu_6I_6 cluster core at both 298 and 77 K, albeit with some marginal variations in its emission wavelengths. Interestingly, an unusual reversal in the mechanochromic luminescent behavior was observed for these isostructural MOFs at 298 K wherein a pronounced blue-shifted high energy emission for **1** (from orange to yellowish-orange) and a red-shifted low-energy emission for **2** (from green to orange) were obtained upon grinding these samples. This is primarily due to the variations in their cuprophilic interactions as **1** displays shorter Cu···Cu distances (2.745(1) Å) in comparison with those present in **2** (3.148(0) Å). As a result, the ground sample of **2** exhibits a prominent red shift in luminescence owing to the reduction of its Cu···Cu distances to an unknown value closer to the sum of van der Waals radii between two Cu(I) atoms (2.80 Å). However, the blue-shifted emission in **1** is presumably attributed to the rise in its lowest unoccupied molecular orbital energy levels caused by changes in the secondary packing forces. Furthermore, the absorption and emission characteristics of **1** and **2** were substantiated by time-dependent density functional theory calculations on their discrete-model compounds. In addition, the syntheses, reactivity studies, and photophysical properties of two one-dimensional MOFs, namely, $\{[MeSi(^3Qy)_3]_2(Cu_2I_2)\}_n$ (**3**) and $\{[MeSi(^3Qy)_3](CuI)\}_n$ (**4**), having dimeric Cu_2I_2 and monomeric CuI moieties, respectively, were examined.

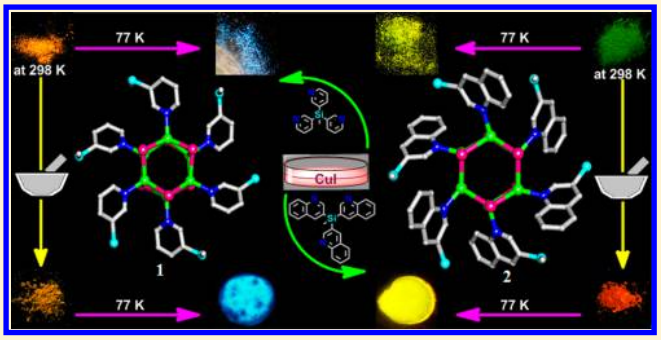

INTRODUCTION

Luminescent coordination compounds have received immense attention in materials science due to their widespread applications in detection and sensing, labeling, and optoelectronic display devices.[1] Metal complexes that exhibit stimuli-responsive luminescent properties are attractive from the standpoint of fundamental understanding and practical applications.[2] Noteworthy examples include the polynuclear complexes of Pt(II), Au(I), and Cu(I) ions, which are shown to exhibit distinct photophysical properties in response to various external stimuli.[3] Thus, they display thermochromism, acidochromism, vapochromism, and mechanochromism (also called piezochromism or tribochromism) in response to the stimuli effects of temperature, pH, solvent vapor, and mechanical grinding, respectively.[4] Such dynamic materials find functional applications such as temperature and pressure sensors, actuators, damage detectors, etc.[5] Donor-stabilized polynuclear clusters of copper(I) halides, particularly copper(I) iodide (CuI), moieties are an important family of compounds in this category.[6] Over the years, these CuI assemblies were obtained in discrete clusters, cages, and in some cases infinite metal–organic framework (MOF) structures and shown to exhibit stimuli-responsive multiple emissions derived from their energetically distinct triplet states.[7] For example, the well-known cubane type $Cu_4I_4(Py)_4$ (Py = pyridyl) cluster shows two unique triplet emissions at room temperature and at 77 K. Thus, at room temperature, it displays a low-energy (LE) cluster-centered (^{3}CC) triplet emission at 580 nm (λ_{ex} = 380 nm) consisting of a mixture of iodide-to-copper charge transfer (^{3}XMCT) and metal d → s,p transitions.[7e] At 77 K, this band disappears, and a new high-energy (HE) band at 438 nm (λ_{ex} = 365 nm) characteristic of iodide-to-ligand charge transfer (^{3}XLCT) and metal-to-ligand charge transfer (^{3}MLCT) transitions was obtained. In another report, the $Cu_4I_4[PPh_2(CH_2CH{=}CH_2)]_4$ cluster, supported by the phosphine ligand, was shown to exhibit both thermochromism and mechanochromism in which the LE ^{3}CC emission was found to be red-shifted by 50 nm upon mechanical grinding.[8] Although the stimuli-responsive behavior of CuI clusters (especially of thermochromism) is fairly studied through various examples, their emission shifts, colors, and shift

Received: September 10, 2014

DOI: 10.1021/ic502207f
Inorg. Chem. XXXX, XXX, XXX–XXX

directions are still unpredictable.[9] In fact, only a limited number of reports are available for the mechanochromic and/or multistimuli-responsive photophysical behavior of CuI-based clusters and MOFs.[10] MOF materials consisting of CuI clusters and organic linkers are an interesting class of compounds as these clusters not only can give rigidity to the framework but also can impart the desired photophysical properties to the framework.[11] Hence, in an effort to synthesize and systematically investigate the multistimuli-responsive behavior of CuI MOFs, we set out to employ the CuI salt in reaction with multisite coordinating ligands based on organosilicon scaffolds. Herein, we report the synthesis and photophysical properties of two isostructural hexameric CuI cluster MOFs, namely, $\{[MeSi(^3Py)_3]_6(Cu_6I_6)\}_n$ (**1**) and $\{[MeSi(^3Qy)_3]_6(Cu_6I_6)\}_n$ (**2**), starting from the N-donor functionalized tridentate arylsilane ligands $MeSi(^3Py)_3$ ($\mathbf{L^1}$) and $MeSi(^3Qy)_3$ ($\mathbf{L^2}$). Use of a main-group element such as silicon as the central atom aids in obtaining identical ligand topologies for various donor functionalities and subsequently has led to the isolation of isostructural CuI MOFs for a systematic investigation of their optical properties. While the MOF **1** displays the usual thermochromism associated with $Cu_4I_4Py_4$ clusters, the MOF **2** shows only the ^{3}XLCT/^{3}MLCT emission due to the Cu_6I_6 cluster core at both 298 and 77 K. More interestingly, an unusual mechanochromic emission behavior was observed for these MOFs wherein a pronounced blue-shifted HE emission for **1** and red-shifted LE emission for **2** was obtained upon mechanical grinding. To the best of our knowledge, this is the first observation for a mechanochromic luminescence umpolung in isostructural CuI clusters mediated by variations in cuprophilic interactions. In addition, the syntheses and photophysical properties of two one-dimensional (1D) MOFs containing dimeric Cu_2I_2 and monomeric CuI moieties were reported in this Paper.

EXPERIMENTAL SECTION

General Remarks. All manipulations were performed under dry atmosphere in standard Schlenk glassware. CuI, $MeSiCl_3$, *n*-BuLi (2.0 M in hexane), 3-bromopyridine, and 3-bromoquinoline were purchased from Aldrich and used as received. NMR spectra were recorded on a 400 MHz Jeol FT spectrometer (^{1}H NMR: 400 MHz, $^{13}C\{^1H\}$ NMR: 100 MHz, ^{29}Si NMR: 80 MHz) at room temperature using $SiMe_4$ as external standards. The powder X-ray diffraction (PXRD) data were obtained from a Bruker-D8 Advance diffractometer. Elemental analyses were performed on a Vario-EL cube elemental analyzer. Fourier-transform infrared (FT-IR) spectra were taken on a PerkinElmer spectrophotometer. The absorption studies were done by a PerkinElmer Lambda 45 UV−visible spectrophotometer; emission and lifetime spectra were recorded on a SPEX Fluorolog HORIBA JOBIN VYON spectrophotometer with a double-grating 0.22 m SPEX 1680 monochromator and a 450 W Xe lamp as the excitation source. The excitation and emission spectra of the complexes were corrected at instrumental function. Thermogravimetric analysis (TGA) data were obtained in PerkinElmer STA 1000 instrument.

Syntheses. $\mathbf{L^1}$: To a stirred solution of 3-bromopyridine (9.48 g, 60 mmol) in dry diethyl ether (80 mL) was added dropwise *n*-butyllithium (4.23g, 66 mmol) at −78 °C, and the mixture was stirred for 1 h to obtain a yellow suspension. Methyltrichlorosilane (2.98 g, 20 mmol) was added to this suspension at −78 °C under nitrogen atmosphere. The reaction mixture was slowly brought back to room temperature and kept stirring for 12 h. The resulting reaction mixture was diluted with diethyl ether (50 mL) and extracted with distilled water (2 × 100 mL). The organic phase was washed with brine solution (2 × 50 mL), dried over Na_2SO_4, and concentrated to yield 4.8 g of clear yellow-red oily product. The crude product was purified through column chromatography using 60% ethyl acetate in hexane to give 3.6 g of $\mathbf{L^1}$ as a white solid (13 mmol, 65%). ^{1}H NMR (400 MHz, $CDCl_3$): δ = 0.92 (s, 3H), 7.29 (m, 3H), 7.74 (dd, 3H), 8.64 (dd, 3H), 8.65 (t, 3H) ppm. $^{13}C\{^1H\}$ NMR (100 MHz, $CDCl_3$): δ 3.92, 123.65, 129.10, 142.73, 151.30, 155.28. ^{29}Si NMR (80 MHz, $CDCl_3$, Me_4Si): δ −12.21 ppm. Matrix-assisted laser desorption ionization time-of-flight mass spectrometry (MALDI-TOF) = 300.0945 $[M + Na]^+$. FT-IR data in powdered sample (cm^{-1}): 1573, 1557, 1474, 1399, 1333, 1258, 1223, 1124, 1027, 813, 717. Anal. Calcd for $C_{16}H_{15}N_3Si$: C, 69.28; H, 5.45; N, 15.15. Found: C, 69.26; H, 5.47; N, 15.18%.

$\mathbf{L^2}$: To a stirred solution of 3-bromoquinoline (6.24g, 30 mmol) in dry diethyl ether (80 mL) was added dropwise *n*-butyllithium (2.11g, 33 mmol) at −78 °C, and the mixture was stirred for 1 h to obtain a brown suspension. Methyltrichlorosilane (1.49 g, 10 mmol) was added to this suspension at −78 °C under nitrogen atmosphere. The reaction mixture was slowly brought back to room temperature and kept stirring for 12 h. The resulting reaction mixture was diluted with diethyl ether (50 mL) and extracted with distilled water (2 × 100 mL). The organic phase was washed with brine solution (2 × 50 mL), dried over Na_2SO_4, and concentrated to yield 3.8 g of clear yellow-red oily product. The crude product was purified through column chromatography using 30% ethyl acetate in hexane to give 3.0 g of $\mathbf{L^2}$ as a yellow-colored oily liquid (70 mmol, 70%). ^{1}H NMR (400 MHz,$CDCl_3$): δ = 1.19 (s, 3H), 7.56 (m, 3H), 7.75 (dd, 3H), 7.78 (m, 3H), 8.14 (dd, 3H), 8.33 (d, 3H), 9.06 (d, 3H) ppm. $^{13}C\{^1H\}$ NMR (100 MHz, $CDCl_3$): δ 3.39, 126.25, 127.39, 127.71, 128.14, 128.30, 129.50, 130.50, 144.95, 148.80, 153.24. ^{29}Si NMR (80 MHz, $CDCl_3$, Me_4Si): δ −11.38 ppm. MALDI-TOF = 450.1235 $[M + Na]^+$. FT-IR data in powdered sample (cm^{-1}): 1718, 1700, 1577, 1570, 1559, 1544, 1541, 1534, 1527, 1522, 1500, 1280, 1108, 789. Anal. Calcd for $C_{16}H_{15}N_3Si$: C, 78.65; H, 4.95; N, 9.83. Found: C, 78.67; H, 4.93; N, 9.80%.

1: To a solution of $\mathbf{L^1}$ (20 mg, 0.07 mmol) in dichloromethane (DCM, 1 mL) kept in a screw-capped vial was added a solution of CuI (41 mg, 0.22 mmol) in acetonitrile (2 mL) with the immediate formation of a yellow precipitate. Then dimethylformamide (DMF, 1 mL) was added to this precipitate and heated at 120 °C under solvothermal condition for 36 h. The resultant solution was slowly cooled to room temperature (at the rate of 0.1 °C/min) to yield colorless crystals of **1**. Yield: 40 mg (65% based on Cu). FT-IR data in KBr pellet (cm^{-1}): 1581, 1559, 1473, 1396, 1334, 1254, 1227, 1194, 1047, 1029, 810, 790, 744, 703. Anal. Calcd for $C_{32}H_{30}Cu_6I_6N_6Si_2$: C, 22.64; H, 1.78; N, 4.95. Found: C, 22.68; H, 1.75; N, 4.93%.

2: To a solution of $\mathbf{L^2}$ (20 mg, 0.046 mmol) in DCM (1 mL) kept in a screw-capped vial was added a solution of CuI (26.7 mg, 0.14 mmol) in acetonitrile (2 mL) with the immediate formation of a yellow precipitate. Then DMF (1 mL) was added to this precipitate and heated at 120 °C under solvothermal condition for 36 h. The resultant solution was slowly cooled to room temperature (at the rate of 0.1 °C/min) to yield yellowish-green colored crystals of **2**. Yield: 30 mg (65% based on Cu). FT-IR data in KBr pellet (cm^{-1}): 1616, 1571, 1490, 1375, 1349, 1263, 1193, 1099, 1021, 909, 862, 750, 656. Anal. Calcd for $C_{56}H_{42}Cu_6I_6N_6Si_2$: C, 33.67; H, 2.12; N, 4.21. Found: C, 33.65; H, 2.15; N, 4.25%.

3: To a solution of $\mathbf{L^2}$ (20 mg, 0.046 mmol) in DCM (1 mL) kept in a screw-capped vial was added a solution of CuI (8.7 mg, 0.046 mmol) in acetonitrile (5 mL) with the immediate formation of a yellow precipitate. Then DMF (1 mL) was added to this precipitate and stirred for 12 h at room temperature. The cloudy solution was filtered, and the filtrate was concentrated to a volume of approximately 2 mL. Reddish-orange crystals of **3** were isolated from this solution after 5 d. Yield: 9.5 mg (30% based on Cu). FT-IR data in KBr pellet (cm^{-1}): 1706, 1675, 1617, 1570, 1491, 1381, 1349, 1262, 1219, 1150, 1098, 1086, 973, 973, 868, 750, 730, 659. Anal. Calcd for $C_{31}H_{28}CuIN_4OSi$: C, 53.87; H, 4.08; N, 8.11. Found: C, 53.90; H, 4.07; N, 8.13%.

4: To a solution of $\mathbf{L^2}$ (20 mg, 0.046 mmol) in DCM (1 mL) kept in a screw-capped vial was added a solution of CuI (8.7 mg, 0.046 mmol) in acetonitrile (5 mL) with the immediate formation of a yellow precipitate. Then DMF (1 mL) was added to this precipitate and was heated at 120 °C under solvothermal condition for 36 h. The

DOI: 10.1021/ic502207f
Inorg. Chem. XXXX, XXX, XXX−XXX

resultant solution was slowly cooled to room temperature (at the rate of 0.1 °C/min) to yield red colored crystals of **4**. Yield: 21 mg (75% based on Cu). FT-IR data in KBr pellet (cm^{-1}): 1706, 1654, 1617, 1570, 1507, 1492, 1374, 1351, 1103, 1103, 1019, 866, 790, 758, 656. Anal. Calcd for $C_{28}H_{21}CuIN_3Si$: C, ; H, 3.43; N, 6.80. Found: C, 54.45; H, 3.41; N, 6.83%.

Synthesis of **2** from **3** (or **4**): To a suspension of **3** (10 mg, 0.014 mmol) or **4** (10 mg, 0.016 mmol) in DMF (2 mL), a solution of CuI (6.7 mg, 0.035 mmol) in acetonitrile (1 mL) was added, and the resulting mixture was heated at 120 °C under hydrothermal condition for 36 h. The resultant solutions were slowly cooled to room temperature (at the rate of 0.1 °C/min) to yield yellowish-green colored crystals of **2**. Yield: 20% (5.7 mg).

Synthesis of **4** from **2**: To a suspension of **2** (10 mg, 0.005 mmol) in DMF (2 mL), a solution of L^2 (4.27 mg, 0.01 mmol) in DCM (1 mL) was added, and the resulting mixture was heated at 120 °C under solvothermal condition for 36 h. The resultant solutions were slowly cooled to room temperature (at the rate of 0.1 °C/min) to yield red colored crystals of **4**. Yield: 20% (2.8 mg).

Similarly, quantitative conversion of **3** to **4** and **4** to **3** can be achieved by treating their 2 mL DMF suspensions at 120 and 90 °C, respectively, under solvothermal conditions.

Crystallography. Reflections were collected on a Bruker Smart Apex Duo diffractometer at 100 K using Mo Kα radiation (λ = 0.710 73 Å). Structures were refined by full-matrix least-squares against F^2 using all data (SHELX).[12] Crystallographic data for all these compounds are listed in Tables S1 and S2 (Supporting Information). All non-hydrogen atoms were refined aniostropically if not stated otherwise. Hydrogen atoms were constrained in geometric positions to their parent atoms. Some of the aromatic carbon atoms in the structure **3** had slightly bad ellipsoids and hence were refined with equal anisotropic displacement parameters or partial isotropic refinements.

Lifetime Measurements. The luminescent lifetimes of L^1, L^2, **1**, **2**, **3**, and **4** were measured at room temperature (289 K) as well as low temperature (77 K). The room-temperature phosphorescence decay profiles were fitted to bi- or triexponential curves. The 77 K phosphorescence decay profiles were fitted to monoexponential equations. In all the cases the lifetimes were fitted by using the DAS software. Throughout the manuscript, the lifetimes of bi- or triexponential curves were discussed only with respect to the highest lifetimes for the sake of simplicity.

Density Functional Theory Calculations. The density functional theory (DFT) calculations were performed by using Gaussian 09 program package.[13] The B3LYP exchange-correlation functional was used throughout for all calculations.[14] A combination of basis sets, namely, 6-31g(d) for C, H, N, and Si and LANL2DZGEN for Cu and I atoms,[15] were used for the discrete model compounds $\{[MeSiH_2(^3Py)]_6(Cu_6I_6)\}$ (**1a**) and $\{[MeSiH_2(^3Qy)]_6(Cu_6I_6)\}$ (**2a**) to obtain the geometry optimization and time-dependent (TD) DFT calculations for the excitation energies. The calculated absorption spectra and related MO contributions were obtained from the TDDFT output file and gausssum2.2.6.1.[16] The theoretical emission wavelengths of **1a** and **2a** were derived by single-point energy calculations on the optimized triplets as the energy difference between the lowest-energy triplet state and its corresponding singlet state.

RESULTS AND DISCUSSION

Syntheses. The precursor ligands L^1 and L^2 were prepared from the reaction of 3-bromopyridine and 3-bromoquinoline with ^{n}BuLi followed by $MeSiCl_3$, respectively. The ligands were characterized by ^{29}Si NMR, mass spectroscopy, emission spectra, and crystallography in case of L^1 (Figures S1–S5, Supporting Information). Crystals of the cluster MOFs **1** and **2** were obtained by the respective reaction of L^1 and L^2 with 3 equiv of copper(I) iodide at 120 °C under solvothermal conditions. Single-crystal XRD analysis revealed that both **1** and **2** were obtained as two-dimensional (2D) assemblies consisting of isostructural hexameric Cu_6I_6 clusters. Use of lower equivalents of the metal salt (CuI) in reaction with L^2 gave 1D assemblies having smaller cluster motifs. Thus, the 1:1 reaction of L^2 and CuI at room temperature (RT) and under solvothermal conditions led to the formation of 1D MOFs $\{[MeSi(^3Qy)_3]_2(Cu_2I_2)\}_n$ **3** and $\{[MeSi(^3Qy)_3](CuI)\}_n$ **4**, respectively. In fact, **3** is the only compound at RT for all the three stoichiometries. Interestingly, treatment of **3** and **4** with added equivalents of CuI gave rise to the 2D MOF **2**. Similarly, by increasing the ligand stoichiometry in **2**, clean products of **3** and **4** can be obtained under solvothermal conditions at different temperatures. However, the reaction of L^1 and CuI in all the three stoichiometries at RT as well as under solvothermal conditions results only in the hexameric MOF **1** (Scheme 1). TGA data show that the MOFs **1** and **2** exhibit stabilities above 300 °C, while **3** and **4** start to decompose at ~115 and 210 °C, respectively (Figure S6, Supporting Information).

Scheme 1. Reaction Schemes and Conditions for the Formation of the CuI Cluster MOFs 1–4

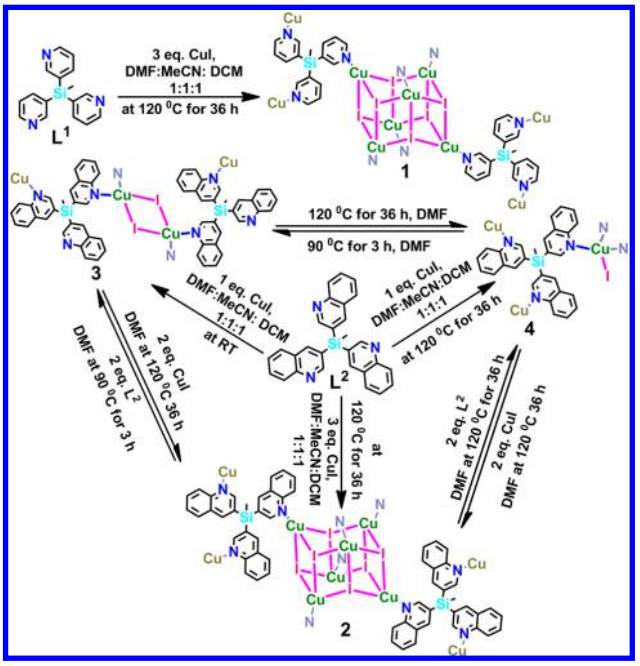

Crystal Structures. The molecular structures of **1** and **2** were solved in hexagonal space groups $R\bar{3}c$ and $R\bar{3}$, respectively (Figure 1a,b and Supporting Information, Figures S7 and S8). The asymmetric unit in both of them consists of one Cu(I) ion, one iodide ion, and one-third of the ligand moiety. The molecular core of **1** and **2** consists of a hexameric Cu_6I_6 cluster in which each I^- ion acts as a μ_3-bridging unit. The Cu(I) ions are located in a tetrahedral coordination consisting of three I^- contacts and one aryl silane N-donor contact. While the Cu_6I_6 clusters, surrounded by the six tripodal ligand segments, act as six-connected nodes, the tridentate silane ligands act as three-connected nodes and associate with three hexameric clusters. The cumulative effect of these interactions is the formation of a 2D hexagonal sheet structure with the topology of a "gra" net (Figure 1c).[17] The adjascent sheets in **1** are further connected by moderately stronger $\pi\cdots\pi$ interactions (4.105(1) Å) between the ^{3}Py moieties in addition to a slightly longer intrasheet $\pi\cdots\pi$ interaction (4.136(0) Å) (Figure S9, Supporting Information).

DOI: 10.1021/ic502207f
Inorg. Chem. XXXX, XXX, XXX–XXX

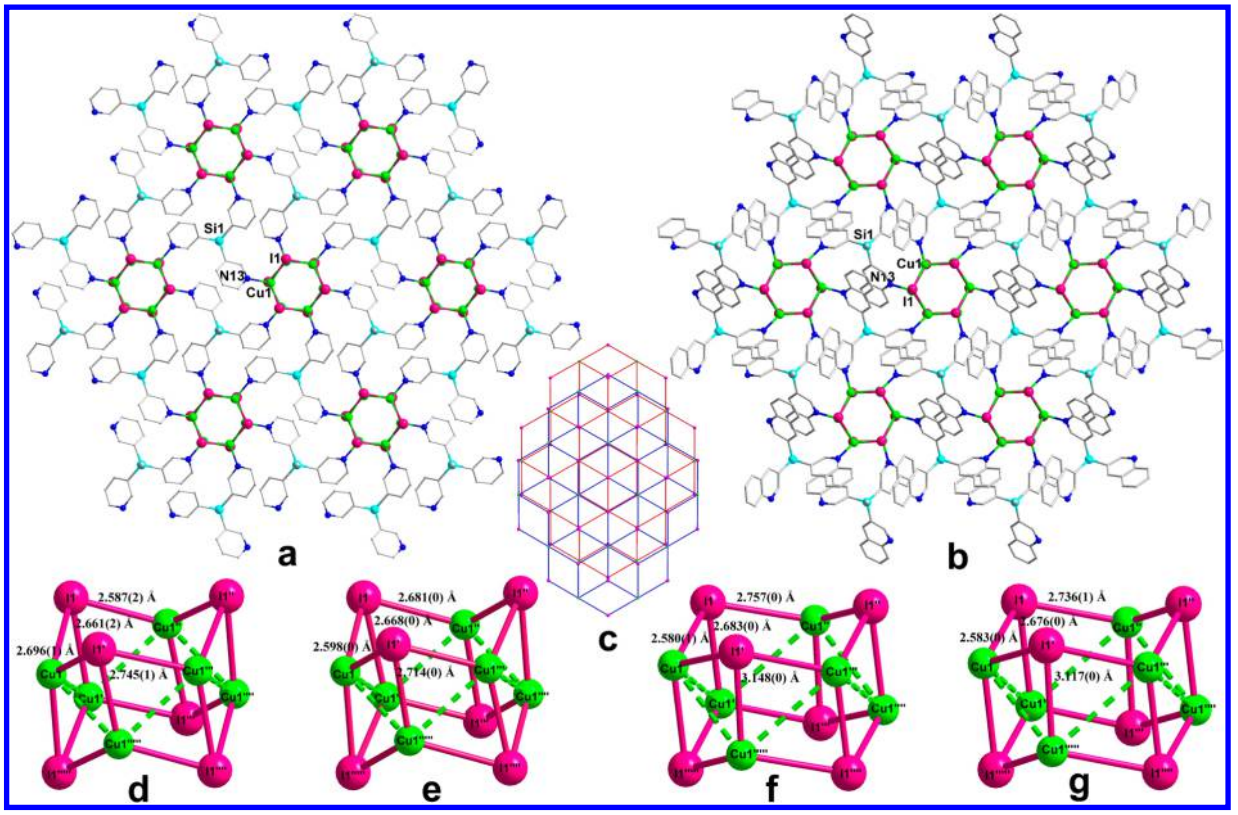

Figure 1. (a) Molecular structures of the hexagonal MOFs (a) **1** and (b) **2**. (c) Topological view of the hexameric sheets in **1** and **2**. View of the Cu_6I_6 core and the Cu···Cu and Cu−I contact distances in **1** at (d) 298 and (e) 100 K and in **2** at (f) 298 and (g) 100 K.

Further, moderate intrasheet C−H···π interactions have been found in **1** (d: 3.467(0) Å, <: 133.64°). However, such interactions are very weak in **2** as it exhibits a longer intrasheet π···π stacking (4.436(1) Å) between the ^{3}Qy moieties, and the shortest C−H···π distance observed in it is at a distance of 4.208(1) Å (Figures S10−S12, Supporting Information). The unit-cell packing diagrams in **1** and **2** reveal the presence of a densely packed structure with almost no void space present in either of them. Although **2** is slightly porous compared to **1**, the measured contact surface and the solvent-accessible volumes of ~205 Å^3 (4.5% of unit-cell volume) and ~12 Å^3 (<1% of unit cell volume), respectively, are very small to accommodate any guest solvent in its solid-state packing.

The crystal structures of **3**·2DMF and **4** were obtained in the triclinic, P-1 and monoclinic, $P2_1/n$ space groups, respectively (Figures 2 and 3 and Supporting Information, Figures S13−S15). The molecular structure of **3** consists of a dimeric Cu_2I_2 core and two bridging ligand scaffolds of $\mathbf{L}^2$ on either sides of it.

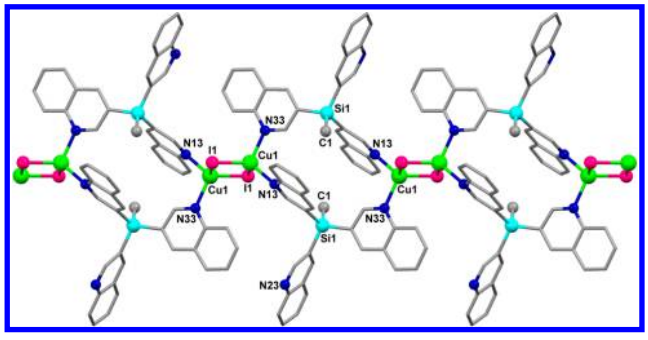

Figure 2. Molecular structure of the 1D MOF **3**.

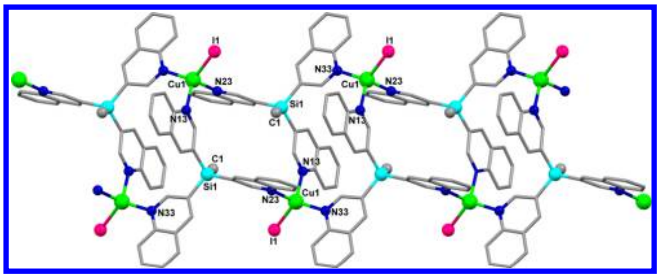

Figure 3. Molecular structure of the 1D MOF **4**.

The ligand $\mathbf{L}^2$ in **3** acts as a bidentate cisoidal ligand (with respect to the Si−Me group) and connects the adjacent Cu_2I_2 segments leading to the formation of a 1D chain polymer. The third ^{3}Qy moiety is noncoordinating and remains above and below the 1D polymer.

The core structure in **4** consists of a monomeric CuI motif connected by the three N-donor sites of the ligand $\mathbf{L}^2$. The Cu(I) atoms are bonded to the three ^{3}Qy segments originating from three different ligands and one terminal iodide ion. Each ligand is attached to three Cu(I) centers in a pseudo C_3-symmetric fashion and help the molecule to propagate in a 1D polymeric structure.

Photophysical Properties. The respective crystals of **1** and **2** are white and pale green solids at ambient temperature, which under UV excitation shows orange and green colored emissions (Figure 4a,b,g,h). When they are cooled to 77 K, MOF **1** shows a bluish emission and MOF **2** shows an intense yellow emission in the solid state (Figure 4c,i). The original emission colors of **1** and **2** can be recovered again within 2 min upon gradually warming the sample to room temperature,

DOI: 10.1021/ic502207f
Inorg. Chem. XXXX, XXX, XXX−XXX

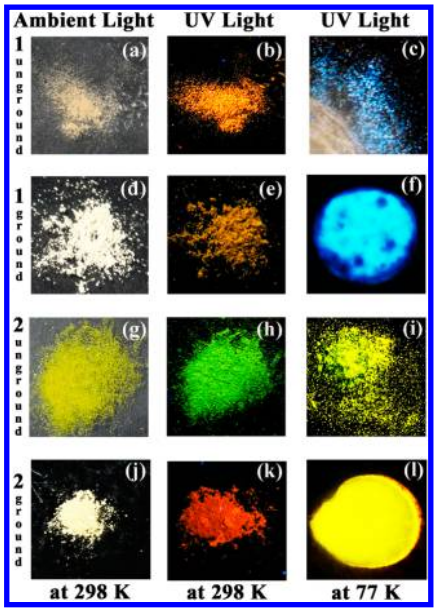

Figure 4. Solid-state emission colors of various samples of **1** and **2** under ambient light and UV lamp (irradiated at 365 nm).

indicating a completely reversible thermochromic luminescence in both of them.

To understand these phenomena further, the excitation and emission spectra of **1** and **2** were recorded in the solid state, and the corresponding results are summarized in Table 1. At 298 K, the emission spectrum of **1** displays an intense LE emission band centered at 611 nm along with a weak HE band at 478 nm (λ_{ex} = 395 nm, Figure S16, Supporting Information). This LE band is in agreement with the orange emission observed at room temperature, which can be attributed to the "cluster-centered" (^{3}CC) emission band characteristic of the traditional $Cu_4I_4L_4$ clusters, while at 77 K the HE band at 478 nm (λ_{ex} = 375 nm) is prominently observed with the concomitant quenching of the ^{3}CC-LE band (Figure 5). This HE band is attributed to the ^{3}XLCT/^{3}MLCT transitions similar to those observed for the cubane-type $Cu_4I_4L_4$ clusters. The decay measurements in **1** at 298 and 77 K gave the lifetime (τ_{em}) values of 1.1 and 57 μS, respectively (Figure 6).

Table 1. Photoluminescence Data of Compounds Used in This Study

complex	temp, K	λ_{ex}, nm	λ_{em}, nm	τ_{em}
$\mathbf{1}_{unground}$	298	395	611	0.16 μs
				1.3 ns
				1.1 μs
	77	375	478	57 μs
$\mathbf{1}_{ground}$	298	395	561	0.02 μs
				1.2 μs
				1.2 ns
	77	375	489	34 μs
$\mathbf{2}_{unground}$	298	395	535	0.03 μs
				0.2 μs
				1.2 ns
	77	325	566	55 μs
$\mathbf{2}_{ground}$	298	395	594	0.03 μs
				0.14 μs
				1.9 ns
	77	325	548	75 μs
3	298	390	645	0.03 μs
				1.6 ns
	77	390	645	58 μs
4	298	390	615	0.03 μs
				1.4 ns
	77	390	615	58 μs
L^1	298	310	405	0.8 ns
				4.9 ns
	77	310	395	0.8 ns
L^2	298	310	395	3.4 ns
				1.8 ns
	77	310	395, 495	0.2 μs

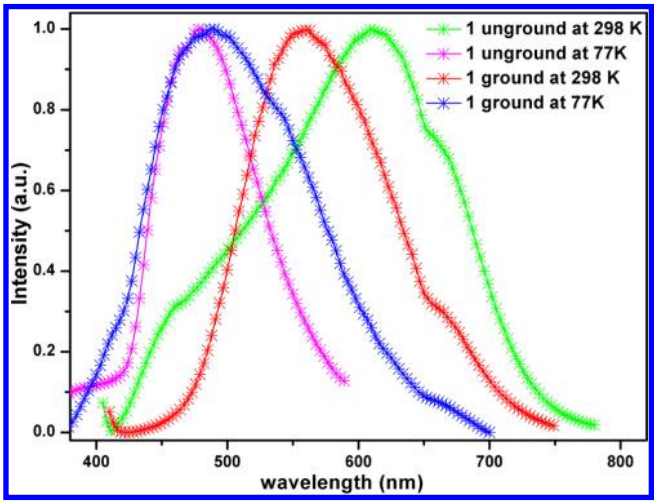

Figure 5. Solid-state photoluminescence spectra of **1** in unground and ground states at 298 and 77 K.

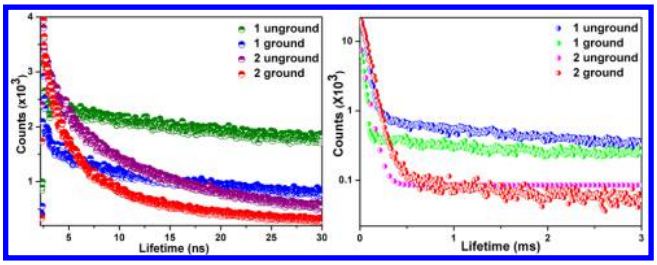

Figure 6. Solid-state phosphorescence decay profiles of **1** and **2** in unground and ground states at 298 K (a) and at 77 K (b).

The emission spectrum of **2** displays a single broad emission band centered at 535 nm (λ_{ex} = 395 nm, Figure S17, Supporting Information) at 298 K, which is red-shifted to 566 nm at 77 K (Figure 7). Although both **1** and **2** are isostructural, the emission maxima in them differ by a large factor owing to the disparate Cu−Cu distances present in these two compounds. Thus, at 298 K, the observed Cu···Cu (average) distances in **1** and **2** are 2.745(1) and 3.148(0) Å, respectively (the van der Waals radii of Cu(I) is 2.80 Å). These values were found to be marginally lowered at 100 K: 2.714(0) Å in **1** and 3.117(0) Å in **2**. Thus, the origin of the emission signatures in **2** at both 298 and 77 K can be attributed to the ^{3}XLCT/^{3}MLCT transitions and not to the ^{3}CC-transitions, as the Cu···Cu distances in it exceeds 2.80 Å. Though it is rare, there are some examples in literature such as $Cu_4I_4(PPh_3)_4$ and $Cu_4I_4(2\text{-}(C_6H_5)_2CH\text{-}C_5H_4N)_4$ where the ^{3}XLCT/^{3}MLCT

DOI: 10.1021/ic502207f
Inorg. Chem. XXXX, XXX, XXX−XXX

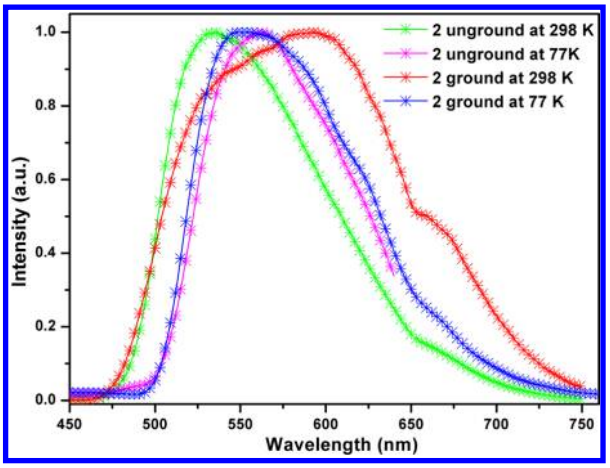

Figure 7. Solid-state photoluminescence spectra of **2** in unground and ground states at 298 and 77 K.

transitions are found to occur at room temperature.[18,7c] Also from the DFT analyses of the ligands and the MOFs (vide supra), which shows the presence of low-lying π^* orbitals for $\mathbf{L}^2$ and **2** (because of their conjugated Qy rings), it is apparent that **2** can exhibit ^{3}XLCT/^{3}MLCT transitions predominantly. Hence it is clear that the higher wavelength ^{3}CC emission in **1** in comparison with lower wavelength ^{3}XLCT/^{3}MLCT transition in **2** is due to the shorter Cu···Cu distances present in **1**.[19,7e] However, upon lowering the temperature to 77 K the emission band in **2** is marginally red-shifted as observed by a slight decrease in its Cu···Cu distances. The measured decay values in **2** showed that the lifetime (τ_{em}) increases from 0.2 to 55 μs as the temperature is switched from 298 to 77 K (Figure 6). The photophysical studies on the 1D MOFs **3** and **4** show no thermochromic behavior that is associated with the 2D MOFs **1** and **2** (Figures S18 and S19, Supporting Information). Thus, the observed ^{3}CC emission bands at 645 and 615 nm in the 298 K luminescence spectra of **3** and **4**, respectively, remained unaltered at 77 K as well (Table 1).

Apart from the thermochromic behavior, the MOFs **1** and **2** exhibit interesting mechanochromic luminescence properties. Upon grinding the sample of **1** in a mortar, the orange emission of **1** was found to be diminished with a dull yellowish-orange emission under the UV lamp (Figure 4d,e). Interestingly, a drastic change of color from green to orange was observed under the UV lamp for **2** during the mechanical grinding (Figure 4h,k and Supporting Information, Figure S20). However, no appreciable color changes were observed for both **1** and **2** under ambient light (Figure 4d,j). The excitation spectra of the respective unground and ground samples of **1** and **2** are closely matching and indicate only minor variations due to temperature or mechanical grinding (Figures S16 and S17, Supporting Information). When the ground samples were treated with 0.5 mL of DMF or DCM (heating at 50 °C or sonication) and dried, the original colors of the samples were recovered. This dynamic behavior of colors was observed for three grinding and solvent recovery cycles confirming the existence of mechanochromism in both of them. To understand whether the mechanical grinding has caused any structural fluctuations, the PXRD analysis was performed for the MOFs **1** and **2** in various states. The PXRD data of the as-synthesized MOFs exhibit well-defined peaks that are in good agreement with the simulated peaks from the single-crystal X-ray data. In contrast, the PXRD of the ground samples of **1** and **2** indicate structural changes in the crushed state when compared to the unit-cell parameters obtained from single-crystal data (Table S3, Supporting Information). A noteworthy feature was the change in cell parameters along all three axes in the crushed form. This could suggest a slipping of the layers with simultaneous increase or decrease in the interlayer distances. However, solvent treatment (as described above) has shown to recover the PXRD patterns due to the pristine samples of **1** and **2** (Figure 8).

Concurrent with these observations, the luminescence band of the ground sample of **1** was found to be blue-shifted to 561 nm (611 nm for the unground sample), while that of the ground sample of **2** was found to be red-shifted to 594 nm (535 nm in the unground state). These changes in emission colors accompanied by large Stoke's shifts confirm the presence of mechanochromism in both of them. Furthermore, the ground sample of **1** exhibits thermochromism and gives rise to the emission due to the ^{3}XLCT/^{3}MLCT transitions at 489 nm upon lowering the temperature to 77 K proving that the Cu_6I_6 core of **1** was not destroyed during mechanical grinding. The luminescence lifetime values of 1.2 and 34 μs obtained for the ground sample of **1** at both 298 and 77 K, respectively, are slightly lower than that of the unground sample of **1** (Figure 6).

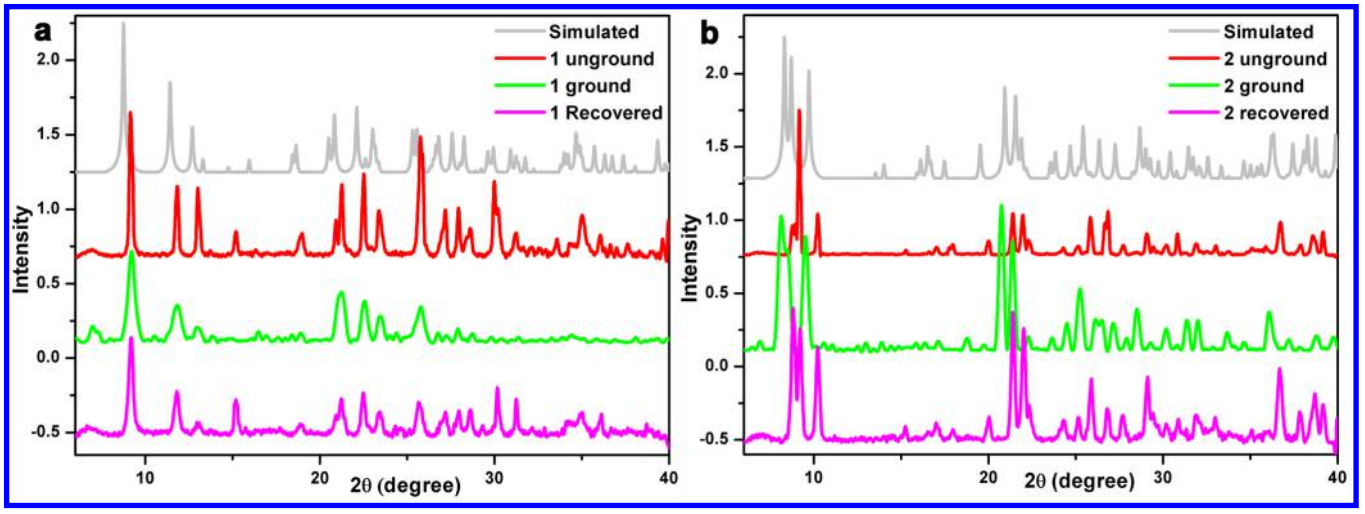

Figure 8. PXRD profiles of unground, ground, and recovered samples of **1** (a) and **2** (b) at 298 K.

DOI: 10.1021/ic502207f
Inorg. Chem. XXXX, XXX, XXX−XXX

Interestingly the ground sample of **2** exhibits a normal thermochromism (77 K), as does **1**, and gives rise to a new blue-shifted luminescence at 548 nm, matching closely with that of the unground sample at 77 K. The decay measurements on $\mathbf{2}_{ground}$ gave lifetime values of 0.14 and 75 μs at 298 and 77 K, respectively (Figure 6). These observations suggest that cuprophilic interactions play a crucial role as the emission bands for the unground and ground samples of **2** at 298 K originate from different triplet states. Thus, grinding the sample of **2** presumably caused a pronounced change in the Cu···Cu distances as observed from the large positive Stoke's shift. Recently, Perruchas and co-workers have shown from the solid-state ^{65}Cu NMR data that mechanical grinding significantly modifies the Cu(I) environment in the local structure of a cubane-type Cu_4I_4 cluster leading to the contraction of its Cu···Cu contacts.[20] Previous DFT calculations on Cu_4I_4 derivatives indicate that the Cu−Cu interactions in the ground state (highest occupied molecular orbital (HOMO)) are non-bonding in character, while the excited state (lowest unoccupied molecular orbital (LUMO)) predominantly has the Cu−Cu bonding character.[21,7b,e] Hence, the origin of the new LE band in $\mathbf{2}_{ground}$ at 594 nm is due to the ^{3}CC transitions caused by the shortening of the Cu···Cu distances by mechanical grinding, while $\mathbf{2}_{unground}$ shows ^{3}XLCT/^{3}MLCT transitions at 298 K. However, at 77 K the ^{3}XLCT/^{3}MLCT transition is seemingly prevalent in the ground and unground samples of **2** resulting in a yellow emission at ∼550 nm in both cases. On the other hand, the Cu···Cu distances observed in $\mathbf{1}_{unground}$ (at both 298 and 77 K) are already below the sum of Cu(I)−Cu(I) van der Waals radii; hence, any shortening of the Cu···Cu distances due to mechanical grinding has little influence in further stabilizing its ^{3}CC excited states. A similar observation can be obtained from the 1D MOF **3**, with the Cu···Cu distance of 2.754(9) Å in the unground state, displaying no change in its emission maxima (645 nm) upon mechanical grinding. Thus, these observations strongly suggest that the possibility of mechanochromism in these Cu_6I_6 clusters may be in other neutral polynuclear Cu_xI_x clusters as well[8,20] and is favored if the Cu···Cu contacts are above the Cu(I) van der Waals radius. However, unlike **2** and other CuI clusters reported before where the emission bands are red-shifted after mechanical grinding, there is a blue shift in emission for the MOF **1**. This could presumably be attributed to the rise in energy level(s) of the LUMO(s) (reduced delocalization of charge) caused by changes in its secondary packing forces such as $\pi\cdots\pi$ and C−H··· π interactions.[22]

Furthermore, the photophysical characteristics of these 2D MOFs were probed by UV−vis spectroscopy and DFT calculations. The solid-state diffuse reflectance (DR) spectra of **1** and **2** show two prominent bands for each of these two compounds: at ∼310 and 395 nm for compound **1** and 310 and 495 nm for compound **2** (Figure S21, Supporting Information). As with most cubane-type $Cu_4I_4L_4$ clusters, the origin of the first high-energy bands are due to ligand $\pi \rightarrow \pi^*$ transitions, while the second low-energy bands are due to the cluster-based ^{1}XLCT/^{1}MLCT transitions. A similar trend was observed when the absorption spectra of these compounds were recorded in DCM suspensions, albeit the presence of multiple absorption shoulders in the ^{1}XLCT region for the MOF **2** (Figures S22 and S23, Supporting Information). To substantiate these observations, preliminary theoretical calculations were performed on the discrete model compounds **1a** and **2a**. The atomic coordinates from the crystal structures of **1** and **2** were taken for these calculations and then were optimized for the gas phase geometries. A detailed examination of the frontier orbitals on the optimized structures of **1a** and **2a** indicates that the majority of the HOMOs (**H**s) were located on the cluster core (up to **H**-53 for **1a** and **H**-33 for **2a**) featuring the iodine (5p) and copper (3d) orbitals, while most of the LUMOs (**L**s) were comprised of the ligand π^* orbitals (up to **L**+11 for **1a** and **L**+11 for **2a**). It is interesting to note that the first few LUMO orbitals in **1a** feature isodensity surfaces on all the six Py chromophores, while in **2a** these are located mostly on a single Qy chromophore. The energy separation between the **H** and **L** orbitals in **1a** and **2a** are found to be 3.74 and 3.02 eV, respectively (Figure 9).

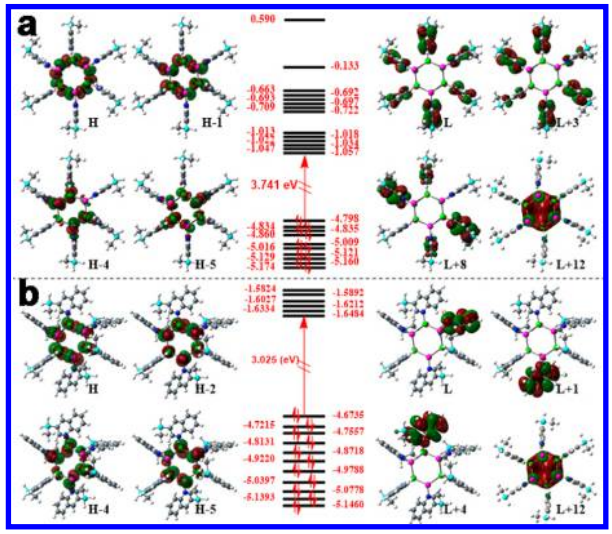

Figure 9. DFT-derived surface diagrams and energies (in eV) of some relevant molecular orbitals at the S_0 optimized geometry for **1a** (a) and **2a** (b).

The optical properties of the discrete model compounds **1a** and **2a** were further examined by TDDFT calculations, and the first 50 transitions were computed. Thus, for **1a**, prominent transitions were found between 352 and 348 nm with major contributions from **H**-1 → **L**+10 (f = 0.018), **H** → **L**+8 (f = 0.017), **H**-5 → **L**+3 (f = 0.014), **H** → **L**+9 (f = 0.013) and **H**-6 → **L** (f = 0.01) transitions (Table S4, Supporting Information). These transitions are closely comparable to the observed ^{1}XLCT/^{1}MLCT band centered at 350 nm in DR spectrum of **1**. Interestingly for **2a**, a wide range of bands were found to occur between 500 and 425 nm with major contributions from **H** → **L**+1 (f = 0.003), **H**-1 → **L** (f = 0.0035), **H** → **L** (f = 0.0035), **H**-2 → **L**+1 (f = 0.0051) **H**-2 → **L**+4 (f = 0.0065), **H**-4 → **L**+4 (f = 0.0065), and **H**-5 → **L**+5 (f = 0.005) transitions (Table S5, Supporting Information, f = oscillator strength). Many of these theoretically predicted transitions closely match with the prominent absorption bands at 478, 460, and 420 nm in the experimental UV−vis spectrum of **2** in DCM suspensions. The additional bands at 382 and 525 nm in the solution (DCM suspension) emission spectrum of **2** were not assigned with any transitions as these regions were not covered in the first 50 TDDFT computed transitions.

To understand the multiple emission properties of **1** and **2**, triplet state optimizations were performed on **1a** and **2a** by following the approach by De Angelis and co-workers.[19b] Promotion of an electron in the ligand-based π^* LUMO in the

DOI: 10.1021/ic502207f
Inorg. Chem. XXXX, XXX, XXX−XXX

S_0 state gives rise to one of the triplet states T_2. The molecular orbitals of **1a** and **2a** in this state closely match with their corresponding S_0 optimized state except that the Cu···Cu distances in them have significantly elongated in the T_2 state (Table S6 and S7, Supporting Information). The emission wavelength from this state, as the adiabatic $S_0 \rightarrow T_2$ gap, can be computed by a single point calculation (Figure S24, Supporting Information). Thus, for **1a** and **2a** these values were computed to be 499 and 578 nm, respectively, matching closely with the observed 77 K emission bands of **1** (478 nm) and **2** (565 nm) corresponding to ^{3}XLCT/^{3}MLCT transitions. The other triplet state T_1, which corresponds to the promotion of an electron in the cluster-based **L**+12 of the singlet ground state S_0. To access this T_1 state we performed separate optimization processes by progressively reducing Cu···Cu distances in the starting geometry. Thus, for **1a**, the cluster-based LUMO is lowered from **L**+12 to **L**+5 and **L**+2 upon reducing the Cu···Cu distances from ∼2.75 Å (singlet optimized) to 2.65 (also 2.60 and 2.55 Å) and 2.50 Å, respectively. However, we were unable to bring this to the desired lowest level of **L** even at a distance of 2.50 Å, which precludes the computation of the observed 298 K ^{3}CC emission wavelength of **1**.

CONCLUSION

In conclusion, by adopting a similar ligand backbone two isostructural MOF materials featuring Cu_6I_6 clusters have been synthesized and studied for their stimuli-responsive photophysical properties. In spite of their isostructural architectures, the MOF **2** exhibits a pronounced mechanochromic behavior compared to **1** showing a drastic change of emission color from green to intense orange. This is attributed to contraction of its Cu···Cu distances to an unknown value closer toward the sum of Cu(I) van der Waals radii. This observation was further substantiated by the emission properties of the 1D MOF **3** (Cu···Cu distance: 2.741(9) Å) in which no change in emission color was observed upon mechanical grinding. However, the MOF **1**, featuring shorter Cu···Cu contacts (below 2.80 Å), exhibits a slightly blue-shifted emission upon mechanical grinding due to changes in secondary packing forces caused by change in unit-cell parameters. Furthermore, interesting thermochromic behavior has been observed for both **1** and **2** in the ground and unground states as the temperature is lowered to 77 K. The present work demonstrates that CuI-containing cluster MOFs can display the multistimuli-responsive photophysical behaviors that are associated with certain discrete Cu_xI_x clusters. Also, it has been shown that by bringing subtle variations in the ligand backbone it is possible to tune the cuprophilic interactions in isostructural CuI MOFs, and thereby their photofunctional behavior can be altered. Stimuli-responsive MOFs featuring CuI cores are a class of smart photoactive materials and have potential utility in modern optoelectronic devices.

ASSOCIATED CONTENT

Supporting Information

X-ray crystallographic data for $\mathbf{L}^1$, **1**, **2**, **3**, and **4** in the CIF format. Tables of bond lengths and angles, TDDFT-computed spectral transitions, illustration of synthetic scheme of $\mathbf{L}^1$ and $\mathbf{L}^2$. ^{29}Si NMR spectra. Illustrated structures. UV−vis, emission, and excitation spectra, TGA measurements, photographs of **2** under ambient light and UV irradiation. Simplified energy level diagram of **1a** cluster. This material is available free of charge via the Internet at http://pubs.acs.org.

AUTHOR INFORMATION

Corresponding Author

*E-mail: boomi@iiserpune.ac.in.

Notes

The authors declare no competing financial interest.

ACKNOWLEDGMENTS

This work was supported by the Department of Science and Technology, India through Grant No. SR/S1/IC-50/2012 (R.B.) and IISER, Pune. M.S.D. thanks the UGC, India, and A.Y. thanks CSIR, India, for the research fellowships. We thank Dr. R. Vaidhyanathan for help with PXRD analysis. We acknowledge Dr. A. Venkatanathan and IISER, Pune, for providing computational facilities.

DEDICATION

This paper is dedicated to Prof. H. W. Roesky on the occasion of his 80th birthday.

REFERENCES

(1) (a) Pang, J.; Marcotte, E. J. P.; Seward, C.; Brown, R. S.; Wang, S. *Angew. Chem., Int. Ed.* **2001**, *40*, 4042−4045. (b) Keefe, M. H.; Benkstein, K. D.; Hupp, J. T. *Coord. Chem. Rev.* **2000**, *205*, 201−228. (c) Fernández-Moreira, V.; Thorp-Greenwood, F. L.; Coogan, M. P. *Chem. Commun.* **2010**, *46*, 186−202. (d) McLaurin, E. J.; Vlaskin, V. A.; Gamelin, D. R. *J. Am. Chem. Soc.* **2011**, *133*, 14978−14980. (e) Cui, Y.; Xu, H.; Yue, Y.; Guo, Z.; Yu, J.; Chen, Z.; Gao, J.; Yang, Y.; Qian, G.; Chen, B. *J. Am. Chem. Soc.* **2012**, *134*, 3979−3982. (f) Uchiyama, S.; Kawai, N.; de Silva, A. P.; Iwai, K. *J. Am. Chem. Soc.* **2004**, *126*, 3032−3033.

(2) (a) Wojtecki, R. J.; Meador, M. A.; Rowan, S. J. *Nat. Mater.* **2011**, *10*, 14−27. (b) Sagara, Y.; Kato, T. *Nat. Chem.* **2009**, *1*, 605−610. (c) Schneider, H. J.; Tianjun, L.; Lomadze, N. *Angew. Chem., Int. Ed.* **2003**, *42*, 3544−3546. (d) Ikeda, T.; Mamiya, J. i.; Yu, Y. *Angew. Chem., Int. Ed.* **2007**, *46*, 506−528.

(3) (a) Huang, L.-M.; Tu, G.-M.; Chi, Y.; Hung, W.-Y.; Song, Y.-C.; Tseng, M.-R.; Chou, P.-T.; Lee, G.-H.; Wong, K.-T.; Cheng, S.-H. *J. Mater. Chem. C* **2013**, *1*, 7582−7592. (b) Choi, S. J.; Kuwabara, J.; Nishimura, Y.; Arai, T.; Kanbara, T. *Chem. Lett.* **2012**, *41*, 65−67. (c) Ni, J.; Zhang, X.; Wu, Y. H.; Zhang, L. Y.; Chen, Z. N. *Chem.—Eur. J.* **2011**, *17*, 1171−1183. (d) Abe, T.; Itakura, T.; Ikeda, N.; Shinozaki, K. *Dalton Trans.* **2009**, 711−715. (e) Kozhevnikov, V. N.; Donnio, B.; Bruce, D. W. *Angew. Chem., Int. Ed.* **2008**, *47*, 6286−6289. (f) Catalano, V. J.; Horner, S. J. *Inorg. Chem.* **2003**, *42*, 8430−8438. (g) Schneider, J.; Lee, Y.-A.; Pérez, J.; Brennessel, W. W.; Flaschenriem, C.; Eisenberg, R. *Inorg. Chem.* **2008**, *47*, 957−968. (h) Ito, H.; Saito, T.; Oshima, N.; Kitamura, N.; Ishizaka, S.; Hinatsu, Y.; Wakeshima, M.; Kato, M.; Tsuge, K.; Sawamura, M. *J. Am. Chem. Soc.* **2008**, *130*, 10044−10045. (i) Lee, Y.-A.; Eisenberg, R. *J. Am. Chem. Soc.* **2003**, *125*, 7778−7779. (j) Laguna, A.; Lasanta, T.; López-de-Luzuriaga, J. M.; Monge, M.; Naumov, P. e.; Olmos, M. E. *J. Am. Chem. Soc.* **2009**, *132*, 456−457. (k) Zhang, J.-X.; He, J.; Yin, Y.-G.; Hu, M.-H.; Li, D.; Huang, X.-C. *Inorg. Chem.* **2008**, *47*, 3471−3473. (l) Dias, H. R.; Diyabalanage, H. V.; Rawashdeh-Omary, M. A.; Franzman, M. A.; Omary, M. A. *J. Am. Chem. Soc.* **2003**, *125*, 12072−12073.

(4) (a) Malwitz, M. A.; Lim, S. H.; White-Morris, R. L.; Pham, D. M.; Olmstead, M. M.; Balch, A. L. *J. Am. Chem. Soc.* **2012**, *134*, 10885−10893. (b) Lefebvre, J.; Batchelor, R. J.; Leznoff, D. B. *J. Am. Chem. Soc.* **2004**, *126*, 16117−16125. (c) Ni, J.; Zhang, L.-Y.; Wen, H.-M.; Chen, Z.-N. *Chem. Commun.* **2009**, 3801−3803. (d) Wadas, T. J.; Wang, Q.-M.; Kim, Y.-j.; Flaschenreim, C.; Blanton, T. N.; Eisenberg, R. *J. Am. Chem. Soc.* **2004**, *126*, 16841−16849. (e) Mínguez Espallargas, G.; Brammer, L.; van de Streek, J.; Shankland, K.; Florence, A. J.; Adams, H. *J. Am. Chem. Soc.* **2006**, *128*, 9584−9585. (f) Zhang, X.; Chi, Z.; Zhang, Y.; Liu, S.; Xu, J. *J. Mater. Chem. C* **2013**,

DOI: 10.1021/ic502207f
Inorg. Chem. XXXX, XXX, XXX−XXX

1, 3376−3390. (g) Shan, X.-c.; Jiang, F.-l.; Yuan, D.-q.; Zhang, H.-b.; Wu, M.-y.; Chen, L.; Wei, J.; Zhang, S.-q.; Pan, J.; Hong, M.-c. *Chem. Sci.* **2013**, *4*, 1484−1489.
(5) (a) Baleizao, C.; Nagl, S.; Schäferling, M.; Berberan-Santos, M. N.; Wolfbeis, O. S. *Anal. Chem.* **2008**, *80*, 6449−6457. (b) Wang, X.-d.; Wolfbeis, O. S.; Meier, R. J. *Chem. Soc. Rev.* **2013**, *42*, 7834−7869. (c) Nagura, K.; Saito, S.; Yusa, H.; Yamawaki, H.; Fujihisa, H.; Sato, H.; Shimoikeda, Y.; Yamaguchi, S. *J. Am. Chem. Soc.* **2013**, *135*, 10322−10325. (d) Sage, I.; Badcock, R.; Humberstone, L.; Geddes, N.; Kemp, M.; Bourhill, G. *Smart Mater. Struct.* **1999**, *8*, 504. (e) Sage, I.; Bourhill, G. *J. Mater. Chem.* **2001**, *11*, 231−245.
(6) Ford, P. C.; Cariati, E.; Bourassa, J. *Chem. Rev.* **1999**, *99*, 3625−3648 and referscences therein.
(7) (a) Ford, P. C.; Vogler, A. *Acc. Chem. Res.* **1993**, *26*, 220−226. (b) Ford, P. C. *Coord. Chem. Rev.* **1994**, *132*, 129−140. (c) Vitale, M.; Palke, W. E.; Ford, P. C. *J. Chem. Phys.* **1992**, *96*, 8329−8336. (d) Xie, H.; Kinoshita, I.; Karasawa, T.; Kimura, K.; Nishioka, T.; Akai, I.; Kanemoto, K. *J. Chem. Phys. B* **2005**, *109*, 9339−9345. (e) Kyle, K. R.; Ryu, C. K.; Ford, P. C.; DiBenedetto, J. A. *J. Am. Chem. Soc.* **1991**, *113*, 2954−2965. (f) Yadav, A.; Srivastava, A. K.; Balamurugan, A.; Boomishankar, R. *Dalton Trans.* **2014**, *43*, 8166−8169. (g) Sun, D.; Yuan, S.; Wang, H.; Lu, H.-F.; Feng, S.-Y.; Sun, D.-F. *Chem. Commun.* **2013**, *49*, 6152−6154. (h) Perruchas, S.; Desboeufs, N.; Maron, S. b.; Le Goff, X. F.; Fargues, A.; Garcia, A.; Gacoin, T.; Boilot, J.-P. *Inorg. Chem.* **2011**, *51*, 794−798.
(8) Perruchas, S.; Goff, X. F. L.; Maron, S.; Maurin, I.; Guillen, F.; Garcia, A.; Gacoin, T.; Boilot, J.-P. *J. Am. Chem. Soc.* **2010**, *132*, 10967−10969.
(9) (a) Wong, F. H.; Banks, D. S.; Abu-Arish, A.; Fradin, C. *J. Am. Chem. Soc.* **2007**, *129*, 10302−10303. (b) Peng, H.; Stich, M. I.; Yu, J.; Sun, L. n.; Fischer, L. H.; Wolfbeis, O. S. *Adv. Mater.* **2010**, *22*, 716−719. (c) Feng, J.; Tian, K.; Hu, D.; Wang, S.; Li, S.; Zeng, Y.; Li, Y.; Yang, G. *Angew. Chem., Int. Ed.* **2011**, *50*, 8072−8076.
(10) (a) Shan, X.-C.; Zhang, H.-B.; Chen, L.; Wu, M.-Y.; Jiang, F.-L.; Hong, M.-C. *Cryst. Growth Des.* **2013**, *13*, 1377−1381. (b) Balch, A. L. *Angew. Chem., Int. Ed.* **2009**, *48*, 2641−2644. (c) Shan, X.-C.; Jiang, F.-L.; Chen, L.; Wu, M.-Y.; Pan, J.; Wan, X.-Y.; Hong, M.-C. *J. Mater. Chem. C* **2013**, *1*, 4339−4349.
(11) (a) Gu, X.; Xue, D. *Inorg. Chem.* **2007**, *46*, 5349−5353. (b) Kitagawa, H.; Ozawa, Y.; Toriumi, K. *Chem. Commun.* **2010**, *46*, 6302−6304. (c) Li, M.; Li, Z.; Li, D. *Chem. Commun.* **2008**, 3390−3392. (d) Tzeng, B.-C.; Chang, T.-Y. *Cryst. Growth Des.* **2009**, *9*, 5343−5350. (e) Wang, F.; Yu, R.-M.; Wu, X.-Y.; Lu, C.-Z. *Inorg. Chem. Commun.* **2012**, *19*, 70−72.
(12) Sheldrick, G. M. *Acta Crystallogr.* **2008**, *A64*, 112−122.
(13) Frisch, M. J.; Trucks, G. W.; Schlegel, H. B.; Scuseria, G. E.; Robb, M. A.; Cheeseman, J. R.; Scalmani, G.; Barone, V.; Mennucci, B.; Petersson, G. A.; Nakatsuji, H.; Caricato, M.; Li, X.; Hratchian, H. P.; Izmaylov, A. F.; Bloino, J.; Zheng, G.; Sonnenberg, J. L.; Hada, M.; Ehara, M.; Toyota, K.; Fukuda, R.; Hasegawa, J.; Ishida, M.; Nakajima, T.; Honda, Y.; Kitao, O.; Nakai, H.; Vreven, T.; Montgomery, J. A.; Jr., Peralta, J. E.; Ogliaro, F.; Bearpark, M.; Heyd, J. J.; Brothers, E.; Kudin, K. N.; Staroverov, V. N.; Keith, T.; Kobayashi, R.; Normand, J.; Raghavachari, K.; Rendell, A.; Burant, J. C.; Iyengar, S. S.; Tomasi, J.; Cossi, M.; Rega, N.; Millam, J. M.; Klene, M.; Knox, J. E.; Cross, J. B.; Bakken, V.; Adamo, C.; Jaramillo, J.; Gomperts, R.; Stratmann, R. E.; Yazyev, O.; Austin, A. J.; Cammi, R.; Pomelli, C.; Ochterski, J. W.; Martin, R. L.; Morokuma, K.; Zakrzewski, V. G.; Voth, G. A.; Salvador, P.; Dannenberg, J. J.; Dapprich, S.; Daniels, A. D. *Gaussian 09*, Revision C.01; Gaussian, Inc.: Wallingford, CT, 2013.
(14) Becke, A. D. *J. Chem. Phys.* **1993**, *98*, 5648−5652.
(15) Hay, P. J.; Wadt, W. R. *J. Chem. Phys.* **1985**, *82*, 270−280.
(16) O'boyle, N. M.; Tenderholt, A. L.; Langner, K. M. *J. Comput. Chem.* **2008**, *29*, 839−845.
(17) O'Keeffe, M.; Yaghi, O. M. *Chem. Rev.* **2012**, *112*, 675−702.
(18) (a) Ryu, C. K.; Vitale, M.; Ford, P. C. *Inorg. Chem.* **1993**, *32*, 869−874. (b) Perruchas, S.; Tard, C.; Le Goff, X. F.; Fargues, A.; Garcia, A.; Kahlal, S.; Saillard, J.-Y.; Gacoin, T.; Boilot, J.-P. *Inorg. Chem.* **2011**, *50*, 10682−10692. (c) Kyle, K. R.; Ford, P. C. *J. Am. Chem. Soc.* **1989**, *111*, 5005−5006.
(19) (a) Kim, T. H.; Shin, Y. W.; Jung, J. H.; Kim, J. S.; Kim, J. *Angew. Chem., Int. Ed.* **2008**, *47*, 685−688. (b) De Angelis, F.; Fantacci, S.; Sgamellotti, A.; Cariati, E.; Ugo, R.; Ford, P. C. *Inorg. Chem.* **2006**, *45*, 10576−10584.
(20) Benito, Q.; Le Goff, X. F.; Maron, S. b.; Fargues, A.; Garcia, A.; Martineau, C.; Taulelle, F.; Kahlal, S.; Gacoin, T.; Boilot, J.-P. *J. Am. Chem. Soc.* **2014**, *136*, 11311−11320.
(21) (a) Vitale, M.; Ryu, C. K.; Palke, W. E.; Ford, P. C. *Inorg. Chem.* **1994**, *33*, 561−566. (b) Vega, A.; Saillard, J.-Y. *Inorg. Chem.* **2004**, *43*, 4012−4018. (c) Mealli, C.; Godinho, S. S.; Calhorda, M. J. *Organometallics* **2001**, *20*, 1734.
(22) (a) Chung, J. W.; You, Y.; Huh, H. S.; An, B.-K.; Yoon, S.-J.; Kim, S. H.; Lee, S. W.; Park, S. Y. *J. Am. Chem. Soc.* **2009**, *131*, 8163−8172. (b) Mizukami, S.; Houjou, H.; Sugaya, K.; Koyama, E.; Tokuhisa, H.; Sasaki, T.; Kanesato, M. *Chem. Mater.* **2005**, *17*, 50−56. (c) Crenshaw, B. R.; Weder, C. *Chem. Mater.* **2003**, *15*, 4717−4724. (d) Tzeng, B. C.; Chang, T. Y.; Sheu, H. S. *Chem.—Eur. J.* **2010**, *16*, 9990−9993. (e) Kojima, M.; Taguchi, H.; Tsuchimoto, M.; Nakajima, K. *Coord. Chem. Rev.* **2003**, *237*, 183−196.

DOI: 10.1021/ic502207f
Inorg. Chem. XXXX, XXX, XXX−XXX